©2005 Society of Economic Geologists, Inc.
Economic Geology, v. 100, pp. 1529–1545

Mixing of Sodic and Calcic Brines and Uranium Deposition at McArthur River, Saskatchewan, Canada: A Raman and Laser-Induced Breakdown Spectroscopic Study of Fluid Inclusions

Donatienne Derome, Michel Cathelineau,† Michel Cuney, Cécile Fabre, Thérèse Lhomme,

CREGU and UMR CNRS-7566 G2R, BP239-54506 Vandoeuvre les Nancy cedex, France

and David A. Banks

School of Earth Science, University of Leeds, Leeds LS2 9JT, United Kingdom

Abstract

The richest U deposit in Saskatchewan, Canada, occurs in the McArthur River area, in the vicinity of the unconformity between the Athabasaca sandstones and an Archean to lower Proterozoic basement. Paleofluids related to the silicification of the sandstones and the formation of pre- and postore cements in breccias were studied using microthermometry, Raman microspectroscopy, and laser induced breakdown spectroscopy (LIBS) on individual fluid inclusions. A detailed reconstruction of the fluid composition in the system Na-Ca-Mg-Cl shows that two types of brines are responsible for the main quartz cements: an NaCl-rich brine (25 wt % NaCl, up to 14 wt % $CaCl_2$, and up to 1 wt % $MgCl_2$), which is interpreted as a primary formation water that was expelled from bedded evaporites; and a $CaCl_2$-rich brine (5–8 wt % NaCl, 20 wt % $CaCl_2$, and up to 11 wt % $MgCl_2$), which is considered to have formed during the interaction between the NaCl-rich brine and Ca-rich minerals in the basement and was introduced into the fault system and mixed with the NaCl-rich brine during the critical stage of U deposition. The pressure-temperature conditions of formation of the quartz cements are estimated to be 1,200 to1,400 bars and 190° to 235°C for the silicification events during the preore stage, and 500 to 900 bars after a pressure decrease from lithostatic conditions and slightly lower temperatures due to the mixing of the NaCl-rich brine with the cooler (approx 140°C) $CaCl_2$-rich brine during the main stage of breccia sealing. Temperature and pressure drops combined with the effects of brine mixing appear to be key factors for the main stages of quartz cementation and U deposition at the McArthur deposit.

Introduction

Unconformity-type uranium deposits are the most profitable source of uranium because of their exceptionally high grade and large tonnage. At least 10 unconformity-type uranium deposits have been discovered in the Athabasca basin, northern Saskatchewan, Canada (Fig. 1), since the Rabbit Lake deposit was discovered in 1968 (Heine, 1986). In unconformity-type uranium deposits, the ore is located close to the intersection of the unconformable contact between Archean to lower Proterozoic metamorphic rocks and a middle Proterozoic sandstone cover with reverse faults that are rooted in the basement in graphitic metasedimentary rocks. Several processes, including supergene (Knipping, 1974) and hydrothermal processes (Little, 1974), have been proposed to account for the formation of the high-grade unconformity-type deposits. However, two genetic models have prevailed. The first model suggests that uranium deposition resulted from mixing between oxidized basinal brines and basement-derived reduced fluids (Pagel, 1975a; Pagel and Jaffrezic, 1977; Hoeve and Sibbald, 1978; Pagel et al., 1980; Hoeve and Quirt, 1987; Wilson and Kyser, 1987; Kotzer and Kyser, 1995; Fayek and Kyser, 1997). The second model proposes that uranium deposition was caused by the interaction of basinal brines with the reduced basement lithologies (Hoeve and Quirt, 1984; Komninou and Sverjensky, 1996; Fayek and Kyser, 1997). Although brines have been documented in

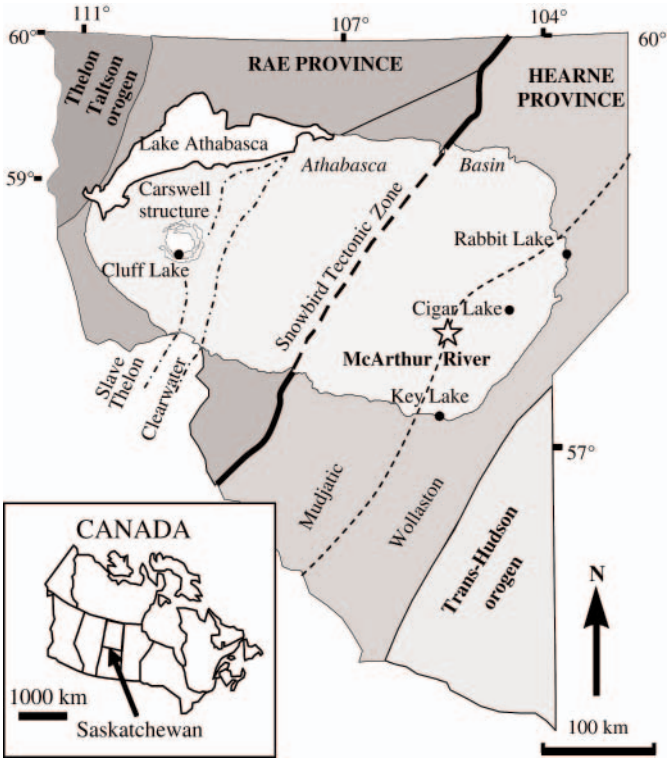


Fig. 1. Location of the main unconformity-type uranium deposits in the Athabasca basin (modified from Ruzicka, 1986).

† Corresponding author: e-mail: michel.cathelineau@g2r.uhp-nancy.fr

previous fluid inclusion studies (Pagel, 1975b; Pagel and Jaffrezic, 1977; Pagel et al., 1980; Kotzer and Kyser, 1995), no fluid compositions were reported. This study adresses four questions concerning the ore-forming fluids: (1) how many fluid types have circulated in the vicinity of the McArthur P2 north orebody and what are their major element compositions? (2) are the brines and the silicification and mineralization events genetically related? (3) do the different fluid types have similar origins? and (4) did the eastern part of the Athabasca basin undergo pressure and temperature variations from diagenesis to the ore-forming event? To answer these questions, a fluid inclusion study of sandstones and basement rocks of the McArthur River deposit was undertaken. This deposit was chosen because of its exceptionally high grade and tonnage (estimated at 198,000 t of contained U_3O_8 at a grade of 25%, in May 2005: www.Cameco.com).

Kotzer and Kyser (1995) reported preliminary fluid inclusion data for this deposit in an overview of the genesis of Athabasca unconformity-type uranium deposits. However, no detailed compositional data, isochors, or pressure-temperature reconstructions of the McArthur River area have been published previously. The relative chronology of the different fluid types, their chronology with respect to mineralization, and their relationship with the mineralogy of the host rocks have been established previously (Derome, 2002). The current study presents detailed compositions of individual fluid inclusions that have been determined by combining microthermometry with in situ analytical techniques (Raman microprobe and laser induced breakdown spectroscopy, LIBS). Finally, a reconstruction of the pressure, temperature, and composition evolution of paleofluids in the vicinity of the McArthur River orebody is proposed, and the possible role of these fluids in the genesis of the deposit is discussed.

Geologic Setting

Regional geology

The Athabasca sedimentary basin unconformably overlies a basement complex of Archean and Paleoproterozoic rocks. The northeast-trending Snowbird tectonic zone separates the basement into two distinct provinces (Hoffman, 1990). Both the Rae province to the west and the Hearne province to the east consist of Archean gneisses, Aphebian (Paleoproterozoic) platform metasedimentary rocks and mafic to felsic plutons (Madore et al., 1999; Thomas et al., 2000; Annesley and Madore, 2003). The Hearne province underwent extensive thermotectonic reworking during the Trans-Hudson orogeny (ca. 1860–1720 Ma; Chiarenzelli et al., 1998; Thomas et al., 2000; Annesley et al., 2001; Annesley and Madore, 2002). Most of the known unconformity-type uranium deposits are located in the eastern part of the Athabasca basin, in the vicinity of the graphite-rich Cable Bay shear zone that occurs between the Mudjatik and the Wollaston domains (Fig.1). The Athabasca basin occurs as a series of northeast-southwest–oriented subbasins controlled by major Hudsonian faults rooted in the basement rocks (Hoeve and Sibbald, 1978; Hoeve and Quirt, 1984; Ramaekers, 1990; Kotzer and Kyser, 1995). These faults were reactivated after the filling of the Athabasca basin (Hoeve and Sibbald, 1978; Kotzer and Kyser, 1995) and have remained active until recent times (Hoeve and Quirt, 1984). This late Paleo- to Mid-Proterozoic basin, which formed at about 1700 to 1750 Ma (Armstrong and Ramaekers, 1985; Kotzer et al., 1992), contains Helikian fluvial to marine quartz-rich sandstone of the Fair Point and Manitou Falls Formations (Ramaekers, 1990; Fayek and Kyser, 1997). The sandstones were deposited in a near-shore, shallow shelf environment (Ramaekers, 1990). They are overlain by marine sandstones, phosphatic siltstones, and phosphatic mudstones of the Lazenby Lake and Wolverine Point Formations, which in turn are overlain by sandstones of the Locker Lake, Otherside, and Turma Lake Formations, and finally by shales of the Douglas Formation and stromatolitic carbonates of the Carswell Formation. The last two formations are only preserved around the Carswell structure, which is thought to have originated as a meteorite impact. The filling of the basin is thought to have occurred during several transgressive-regressive cycles (Ramaekers, 1990). Then, the basin was intruded by several northwest-trending mafic dikes, dated at ca.1227 ± 11 Ma by the Rb-Sr method (Armstrong et al., 1988), during post-Athabasca tectonic activity (Fayek and Kyser, 1997). Similar U-Pb ages (1267 ± 2 Ma) were obtained on the MacKenzie diabase dikes (LeCheminant and Heaman, 1989; Thomas et al., 2000), and the two types of intrusions are believed to be linked to a single event (Cumming and Krstic, 1992).

Geology of the McArthur River deposit

The McArthur River deposit occurs in the southeastern part of the Athabasca basin, close to the Cable Bay shear zone (Fig.1). The studied area is the basement-hosted P2 North orebody and its enclosing formations (Fig. 2). In the McArthur River region, an approximately 500-m-thick section of Athabasca sandstone is preserved. The sandstone comprises the four members of the Manitou Falls Formation (from basement to surface, MFa, b, c, and d). The basal part of the MFa contains fanglomerates (Quirt, 2000). The overlying sandstone is affected by an early silicification that commonly preserved hematite between detrital grains and quartz overgrowths (here designated Qz1). Above the mineralization, the sandstones are affected by a postdiagenetic, premineralization pervasive silicification (Qz2). This pervasive silicification is particularly well developed up to 150 m above the P2 orebody and contains numerous drusy quartz veins (Qz3; Matthews et al., 1997; Thomas et al., 2000). The deposit is structurally controlled by the northeast-trending, southeast-dipping, graphite-rich P2 reverse fault. The basement lithologies contain, from east to west (Fig. 2b): (1) biotite-quartz-garnet metapelitic gneisses (hanging wall), (2) a graphite-rich fault zone, (3) garnet-and cordierite-rich ± graphitic pelitic gneisses with local fine-grained banded calcsilicates, pegmatites, and leucogranites (footwall), and (4) feldspathic metaquartzite (McGill et al., 1993; Matthews et al., 1997; Thomas et al., 2000).

The P2 north orebody occurs close to the intersection between the P2 fault and the unconformity between the Athabasca group and the basement. Uranium mineralization occurs mainly in the cordierite-rich metapelites and extends slightly into the sandstone, along the edge of the basement wedge. Brecciation is well developed within and around the orebodies. Most of the mineralization occurs in chlorite-rich

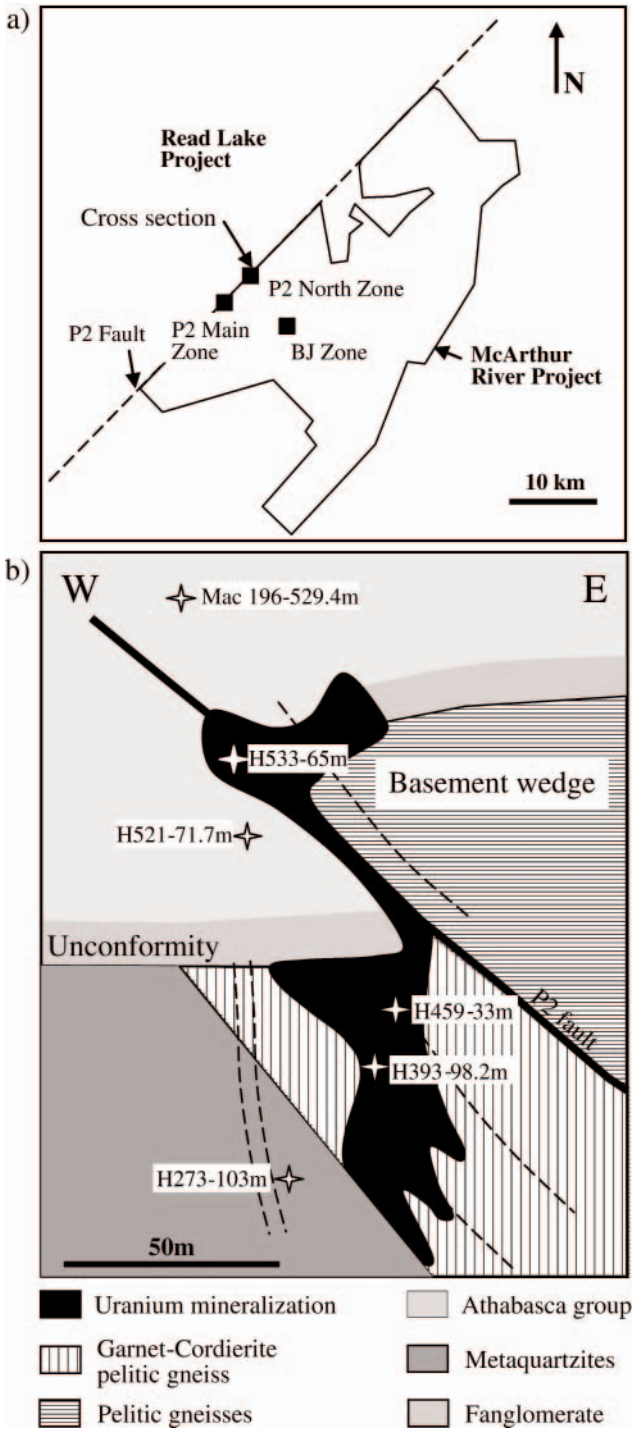


FIG. 2. (a). Location of the McArthur River area. (b). Schematic cross section of the P2 North zone (McArthur River deposit), showing the projection of the approximate location of most of the studied samples (modified from Thomas et al., 2000).

breccias (McGill et al., 1993). These breccias commonly occur as fragments in breccias cemented by drusy quartz and carbonate. Widespread alteration halos are developed around the deposit. Alteration includes intense silicification (Qz2 and Qz3), Mg chlorite (sudoite), Mg tourmaline (dravite), and kaolinite (Thomas et al., 2000). These minerals are attributed to syn- to postmineralizing hydrothermal events (Kotzer and Kyser, 1995; Fayek and Kyser, 1997; Alexandre et al., 2003). Massive uranium mineralization is commonly cut by thin siderite veinlets that are attributed to late meteoric fluids (Kotzer and Kyser, 1995). Previous U-Pb geochronological studies on uranium oxides at McArthur River indicate several stages of uranium deposition and remobilization. The earliest recorded stage at ~1520 Ma (1514 ± 18 Ma: Cummings and Krstic, 1992; 1519 ± 22: Fayek et al., 2002; 1540 ± 38 Ma: Alexandre and Kyser, 2003) represents the minimum age for initial crystallization of uraninite at McArthur River according to Alexandre and Kyser (2003). Younger ages of 1327 ± 8 Ma (Cummings and Krstic, 1992), 1247 ± 88 and 950 ± 27 Ma are interpreted as recrystallization ages (Alexandre and Kyser, 2003).

Sampling and Mineral Paragenesis

Sampling

Samples were taken from hematite-rich and bleached sandstones, as well as from the basement rocks, in and adjacent to the basement-hosted high-grade P2 orebody. Sandstone samples were obtained from the basal MFa Formation. The location of most of the studied samples is indicated in Figure 2b, and a summary of the characteristics of each sample is presented in Table 1.

Mineral paragenesis

A paragenetic sequence of minerals has been established on the basis of field observations and thin and thick section studies (more than 50 sections). This paragenetic sequence also takes into account previously published data on the McArthur River deposit (Fig. 3).

In the sandstones, diagenetic features are represented by Qz1, hematite (Hem1) occurring at the boundary of the detrital quartz grains and their overgrowths, illite and dickite. The first recognizable postdiagenetic fluid-flow event caused the formation of dravite (Drv1) together with Qz2 in the pore spaces of the sandstones (Table 1, Fig. 3). This event appears to have been synchronous with or postdated a weak dissolution event, as suggested by the corrosion of quartz overgrowths. Qz3 was formed as a result of subsequent brittle fracturing. Dravite needles commonly occur on the wall of the quartz veins and are interpreted as a continuation of the postdiagenetic fluid-flow event which formed the assemblage Drv1 + Qz2. The Qz3 described in the present study corresponds to Q2 of Kotzer and Kyser (1995) and Fayek and Kyser (1997). Secondary hematite (Hem2) is frequently observed as red rims in the late growth zones of Qz3 and is particularly well developed in sample Mac 196-529.4m, where pyrite (Py1) formed after euhedral quartz. No other sulfides were observed in this sample. The formation of Qz2 and Qz3 was followed by significant quartz dissolution. Dissolution was associated with the development of chlorite (Chl1) and dravite (Drv2) in the matrix of breccia bodies. The main uranium mineralization (U1 in the present study) is associated with chlorite-dravite breccias and synchronous with massive quartz dissolution (McGill et al., 1993; Lorilleux et al., 2002; Fig. 4d, e, g). A second stage of brecciation occurred, which clearly postdated U1, as indicated by the occurrence of

TABLE 1. Samples from the McArthur River Deposit (P2 North zone) and from the Read Lake Project Included in This Study

Host rock, location	Sample (drill hole no./depth)	Approximate distance to unconformity (m)	Spatial relationship to U mineralization	Mineralogy
Sandstone McArthur River	Mac188-92.2 m	81.6	n.d.	DetrQz, Hem1, Qz1, Drv1, Drv2, Qz3
Sandstone McArthur River	Mac196-529.4 m	42	Close to weak mineralization (0.5 m)	DetrQz, Qz1, Drv1, Qz2, Chl1, Drv2, Qz3, Hem2,Py1
Sandstone McArthur River	H521-71.7 m	n.d.	Weakly mineralized sample, ~10 from high-grade ore	DetrQz, Qz2, Qz3, Chl1, Drv2, U1, Qz4, Chl2
Sandstone McArthur River	H533-65 m	n.d.	In high-grade ore	DetrQz, Qz1, Qz2, Drv1, Drv2, U1
Sandstone Read Lake	RL6-141 m	436	n.d.	DetrQz, Drv 1, Qz1, Qz2, Drv2, Qz3
Metaquartzite McArthur River	H273-103 m	~50	~10 m from high-grade ore	Drv 2, Qz4, Py1
Uranium ore McArthur River	H393-98.2 m	10–20	In high-grade ore	Chl1, Drv2, U1, Qz4
Uranium ore McArthur River	H459-33 m	10–50	In high-grade ore	Chl1, Drv2, U1, Qz4, Hem3, Chl2, Py2, B1, Dol

Notes: Drill holes H521, H533, H173, H393, and H459 correspond to underground holes; Mac188, Mac195, and RL6 correspond to holes drilled from surface; abbreviations: B = bitumen, Chl = chlorite, Dol = dolomite, Drv = dravite, Hem = hematite, Py = pyrite, Qz = quartz, U = uranium oxide (pitchblende or uraninite), n.d = not determined

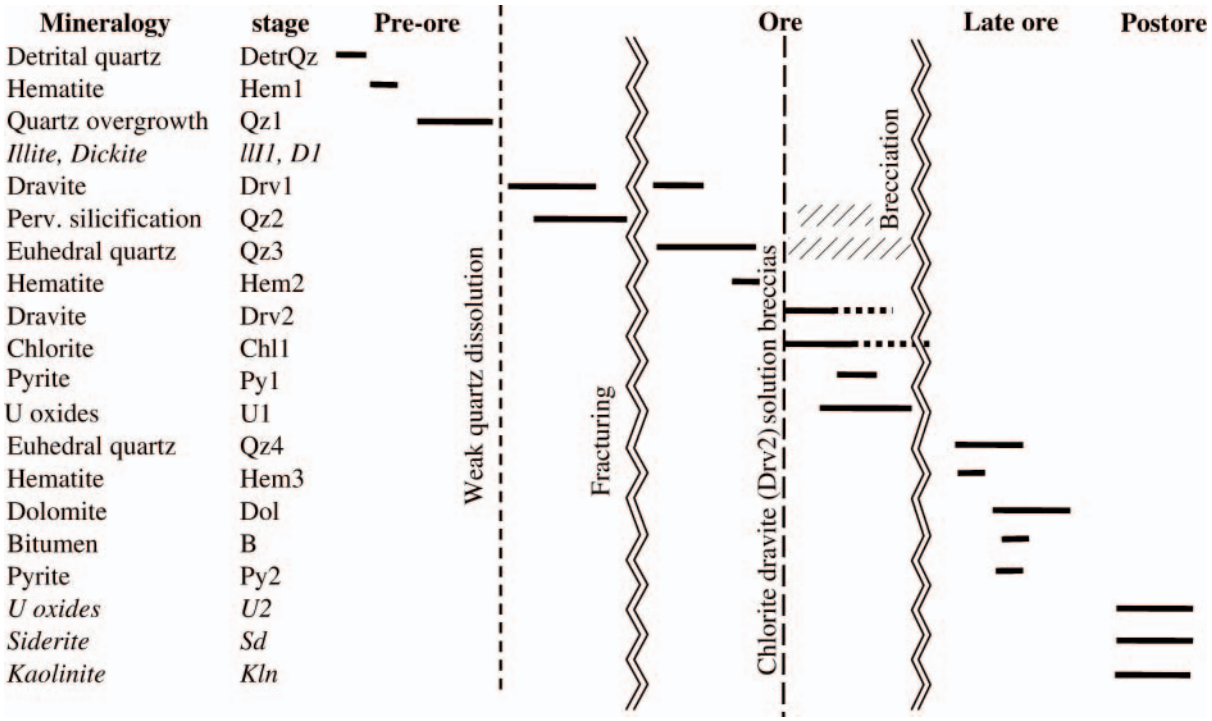


FIG. 3. Summary of the mineral paragenesis in the McArthur River uranium deposit determined from field and thin section observations of the samples from the present study. Data from Kotzer and Kyser (1995) are indicated in italics. Full lines = mineral growth; cross hatch = dissolution. Abbreviations: B = bitumen, Chl = chlorite, D = dickite, Dol = dolomite, Drv = dravite, Hem = hematite, Ill= illite, Kln = kaolinite, Py = pyrite, Qz = quartz, Sd = siderite, U = uranium oxide.

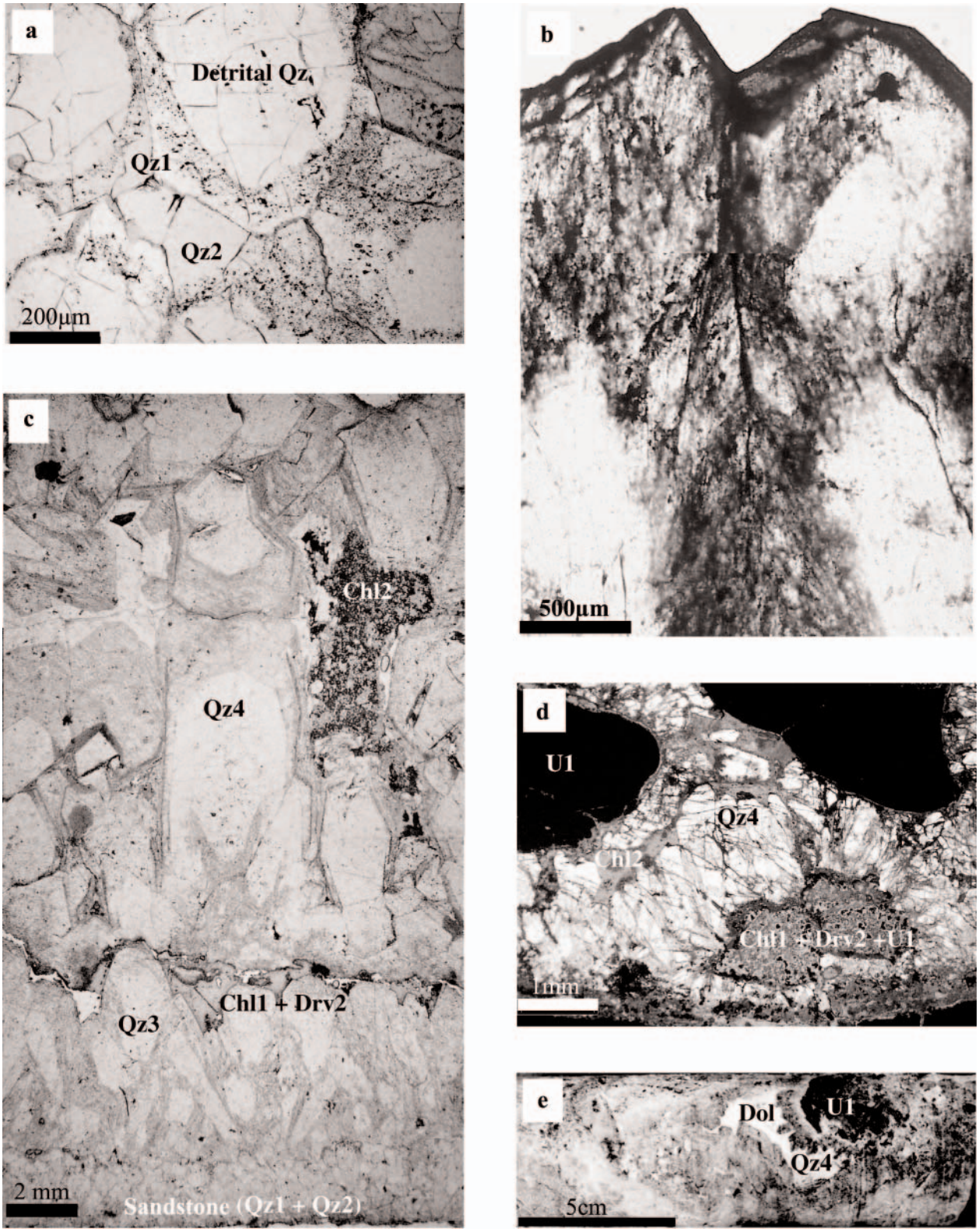


FIG. 4. (a). Sandstone with quartz overgrowths (Qz1) and pervasive silicifications (Qz2); (thin section, transmitted light; Mac 196-529.4m). (b). Primary and pseudosecondary fluid inclusions in euhedral quartz Qz3 in sample H521-71.7m (thick section, transmitted light). (c). Highly silicified sandstone (H521-71.7m), crosscut by a euhedral quartz vein (Qz3) followed by chlorite (Chl1), dravite (Drv2), and euhedral quartz (Qz4) and a second generation of chlorite (Chl2) (thin section, transmitted light). (d). Uranium oxide (U1) in a chlorite (Chl1)-dravite (Drv2) breccia, in turn brecciated and cemented by drusy quartz veins (Qz4) (thin section, transmitted light, sample H393-98.2m). (e). Fragment of pitchblende (U1) in a breccia cemented by quartz (Qz4) and dolomite (Dol) (sample H459-33m).

fragments of chlorite-dravite mineralized breccia. The second-stage breccias were cemented by euhedral quartz Qz4, which locally contains hematite (Hem3) in its last growth zones (sample H459-33m). Dolomite, associated with small bitumen balls, and pyrite fill the residual vugs.

These observations are generally consistent with those of Kotzer and Kyser (1995), Matthews et al. (1997), and Thomas et al. (2000). However, the present study distinguished two generations of euhedral quartz (pre- to synore Qz3 and postore Qz4) according to both petrographic and fluid inclusion studies, whereas the previous studies recognized only one generation of euhedral quartz vein (Q2 of Kotzer and Kyser, 1995; Fayek and Kyser, 1997; and Q1 of Alexandre et al., 2003). The late incursion of meteoric water is represented mainly by late siderite-filled vugs in uranium oxide and kaolinite filling fractures (Kotzer and Kyser, 1995; Fayek and Kyser, 1997). Fluids associated with these late events are not described in the present study.

Fluid Inclusion Study

Methodology

The petrography and relative chronology of fluid inclusions were studied using doubly polished thick sections (300 μm). Microthermometry was carried out on a ®Linkam heating-cooling stage adapted to an ®Olympus microscope to observe ice and hydrate melting, halite dissolution temperatures, and homogenization temperatures (T_h). A ®Labram-Dilor Raman microspectrometer was used at room temperature to determine the composition of the gas phase in fluid inclusions (Dubessy et al., 1989) and to determine the bulk chlorinity of the aqueous phase (Mernagh and Wilde, 1989; Dubessy et al., 2002). Raman microspectroscopy also was used at low temperature to determine the nature of the melting phases (Dubessy et al., 1982; Bakker, 2001). Laser-induced (NdYAG-UV 266nm) breakdown spectroscopy was used to measure cation ratios of the liquid phase of fluid inclusions that were devoid of solids (Fabre et al., 1999). All analyses were performed at the Centre de Recherches sur la Géologie des Matières Premières Minérales et Enérgétiques (CREGU- G2R) in Nancy.

Microthermometry, Raman, and LIBS results

Fluid inclusions were studied in Qz1, Qz2, Qz3, and Qz4 in the sandstone and in Qz4 in the basement rocks (Table 2). The different fluid types present in the fluid inclusions were established on the basis of petrography, microthermometry, chlorinity, and cation ratios, as determined by LIBS analysis. The two main fluid types belong to the H_2O-NaCl-$CaCl_2$ ± $MgCl_2$ system: one fluid end member is an NaCl-rich brine that occurs as two- (liquid, L, vapor, V) or three-phase (L, V, halite) fluid inclusions (denoted Lw and Lwh, Fig. 5a, b); the second end member is a $CaCl_2$-dominated brine occurring as two- (L, V) and three-phase (L,V, halite) fluid inclusions (denoted as Lw and Lwh', respectively, Fig. 5c, d). A third fluid type, which is less common in the vicinity of the McArthur River deposit, consists of a low-salinity fluid that occurs as two-phase (L,V) fluid inclusions with heterogeneous gas/liquid ratios and that is observed only locally in the deposit in fluid inclusion planes in Qz4. The paragenetic relationships between the brines within a single sample are difficult to establish because they occur together in Qz2, Qz3, and Qz4 (Table 2). A summary of the chemical characteristics of each fluid type derived from microthermometry, Raman, and LIBS data is given in Table 3.

NaCl-rich brines (Lw, Lwh)

Lw fluid inclusions have eutectic temperatures that range from –76° to –50°C (Table 2), typical of the H_2O-NaCl-$CaCl_2$

TABLE 2. Summary of Fluid Inclusion Data (microthermometry, Raman, and laser-induced breakdown spectroscopy) Obtained in the Different Quartz Generations

				Microthermometric characteristics			
Quartz generation	F.I. type (n)	F.I. size (μm)	F.I. chronology	Range	Mode	Raman chlorinity (mol/kg H_2O)	Na/Ca (LIBS)
Qz1 (overgrowths)	Lw_1 (11)	<10	Primary (rare)	$-60<T_e<-50$°C $-25<T_{m(ice)}<-19$°C $93.8<T_h<200$°C	–55°C –22.5°C 165°C	n.d.	n.d.
	Lw' (14)	<20	Secondary	$-75<T_e<-58$°C no freezing$<T_{m(ice)}<-31$°C $54<T_h<110$°C	–65°C –35°C few data	n.d.	n.d.
	Lwh' (4)	<20	Secondary	$147< T_{s(NaCl)} <230$°C $70<T_h<148$°C	n.d. few data	n.d.	n.d.
Qz2 (pervasive silicifications)	Lw_2 (4)	<20	? rare	$-58<T_e<-55$°C $-26.8<T_{m(ice)}<-25.7$°C $-7< T_{m(hyd)} <9.5$°C T_h~150°C (1 data)	–55°C –26°C 9.5°C n.d.	n.d.	n.d.
	Lwh' (17)	<20	Primary?	$150< T_{s(NaCl)}<235$°C (n=9) $63<T_h<129$°C	155°C 75°C	n.d.	n.d.
	Lw' (8)	<20	Primary	$-75<T_e<-70$°C (n=5) no freezing$<T_{m(ice)}<-30$°C $58<T_h<127.5$°C	–75°C –45°C 105°C	n.d.	n.d.

TABLE 2. *(Cont.)*

Quartz generation	F.I. type (n)	F.I. size (μm)	F.I. chronology	Microthermometric characteristics Range	Mode	Raman chlorinity (mol/kg H_2O)	Na/Ca (LIBS)
	Lw" (6)	~15	Secondary	T_e~–41°C (3 data) –10.6<$T_{m(ice)}$<–2.2°C T_h : n.d. (H_2+O_2)	 –35°C	n.d.	n.d.
Qz3 (euhedral quartz veins-sandstone)	Lw_1 (4)	~15	Primary ?	T_e~–50°C (3 data) –21.1<$T_{m(ice)}$<–11.2°C T_h~210°C (1 data)	n.d. n.d. n.d.	n.d.	n.d.
	Lw_2 (24)	5–25	Primary and pseudosecondary	–76<T_e<–54°C –28.8<$T_{m(ice)}$<–24°C 0.5<$T_{m(hyd)}$ <18.5°C 71<T_h<185°C	–72°C –25°C 5°C ~150°C	n.d.	n.d.
	Lwh (2)	15	Primary and pseudosecondary	T_e: n.d. –25<$T_{m(ice)}$<–24°C –3.2<$T_{m(hyd)}$ <–1.2°C 206< $T_{s(NaCl)}$<208°C 133<T_h<136°C	n.d.	n.d.	n.d.
	Lw' (30)	5–35	Primary	–75<T_e<–68°C no freezing or –58<$T_{m(ice)}$<–33.5°C 63<T_h<137°C	–72°C no freezing 115°C	6.5	0.5
	Lwh' (31)	5–35	Primary	–77<T_e<–70°C no freezing or –54<$T_{m(ice)}$<–41°C 147< $T_{s(NaCl)}$<235°C 68<T_h<175°C	–74°C –52°C 175°C 105°C	n.d.	n.d.
	Lw" (14)	10–25	Secondary (fluid inclusion planes)	–53<T_e<–40°C –10<$T_{m(ice)}$<–1.6°C T_h: n.d. (decrepitation due to gas)	–52°C –4.5°C	n.d.	n.d.
Qz4 (euhedral quartz)	Lw_1 (2)	15–30	? rare	–55<T_e<–45°C –20<$T_{m(ice)}$<–14°C T_h~220 (1 value)	nd	3–4.5	4.6
	Lw_2 (70)	15–120	Primary	–75<T_e<–50°C –26.5<$T_{m(ice)}$<–20°C 0<$T_{m(hyd)}$ <21.9°C 101.3<T_h<186°C	–55°C –24.5°C 10°C 165°C	5.8–6.5 mode ~ 6	3–7.7 mode ~ 3
	Lwh (10)	15 to 80	Primary	–58<T_e<–52°C –27.7<$T_{m(ice)}$<–25.3°C 8.8<$T_{m(hyd}$ <19.2°C 99.5< $T_{s(NaCl)}$<176.6°C 104<T_h<188°C	–55°C –26°C 15°C 135°C 160°C	6.5	3.8
	Lw' (12)	5–30	Primary ?	–75<T_e<–60°C –51<$T_{m(ice)}$<–39°C 99<T_h<112°C	–70°C –40°C 110°C	6.5	0.5–1.7
	Lwh' (4)	5–30	? Rare	–70<T_e<–60°C –45<$T_{m(ice)}$<–36°C 115< $T_{s(NaCl)}$<141°C 127<T_h<141°C	 few data	6.5	0.8
	Lw" (7)	10–30	Isolated or as clusters	T_e ~ –35°C –10<$T_{m(ice)}$<–3.1°C 150<T_h<270°C (4 values) (frequent decrepitation due to gas)	–35°C –5.5°C ~ 250°C	1.2–2.2	3.7–5

Notes: F.I. = fluid inclusion, LIBS = laser-induced breakdown spectroscopy, n = number of data, T_e = eutectic temperature, $T_{m(ice)}$ = ice melting temperature, $T_{m(hyd)}$ = hydrohalite melting temperature, $T_{s(NaCl)}$ = halite dissolution temperature, T_h = homogenization temperature (temperature of vapor phase disappearance); Lw_1, Lw_2, and Lwh = NaCl-rich brine, Lw' and Lwh' = $CaCl_2$-rich brine, Lw" = low-salinity fluid

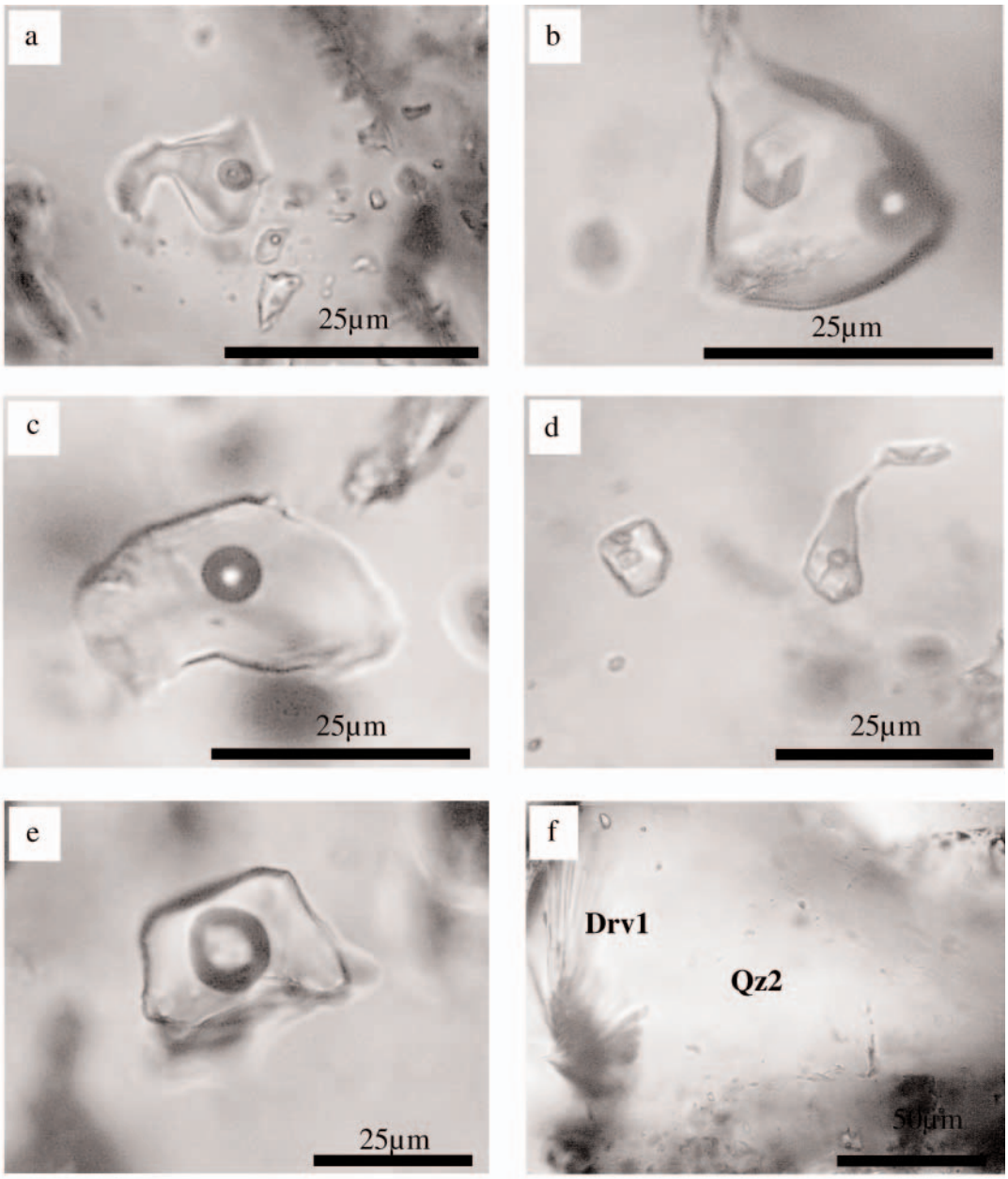


FIG.5. Petrographic characteristics of the different fluid inclusions observed in the McArthur River deposit. (a) Lw, (b) Lwh, (c) Lw', (d). Lwh', (e) Lw", (f) fluid inclusions in Qz2 close to dravites (Drv1).

± $MgCl_2$ system (Roedder, 1984; Oakes et al., 1990; Goldstein and Reynolds, 1994). Lw inclusions are subdivided into Lw_1 and Lw_2 subgroups according to the nature of their last phase to melt during cooling (ice or hydrohalite, respectively).

Lw_1 fluid inclusions were observed mostly in quartz overgrowths (Qz1) of the sandstone (Fig. 6, Table 2). They are also present in other quartz (Qz3 and Qz4) but in lower abundance than in Qz1. Where fluid inclusions are large enough to enable the phase transitions to be observed, the ice-melting temperature $T_{m(ice)}$ values range from –25° to–11.2°C and the T_h values range from 93.8° to 210°C (Fig. 7a, Table 2). Chlorinity ranges from 3 to 4.5 mol/kg H_2O. Due to the size of the fluid inclusions, which are generally smaller than 10 μm in Qz1 (Fig. 5e), or to the presence of trapped solids, only one analysis of an Lw_1 fluid inclusion was carried out by LIBS in a postore drusy quartz crystal Qz4 from the basement. The cation ratios Na/Ca = 4.6 and Ca/Mg = 1 were obtained (Table 2). No gas was detected in the vapor phase of fluid inclusions from Qz1.

In Lw_2 fluid inclusions, the last phase to melt is hydrohalite ($NaCl.2H_2O$) as shown by its Raman spectrum (Dubessy et al., 1982). Lw_2 inclusions mainly occur in Qz4 from the basement and less frequently in Qz2 and Qz3 from the sandstone (Fig. 6, Table 2). Their $T_{m(ice)}$ values range from –21° to –28.8°C, $T_{m(hydrohalite)}$ from –7° to 21.9°C, and T_h from 71.3° to 186°C, with a mode at 165°C. In some cases, hydrohalite

TABLE 3. Summary of Fluid Inclusion Microthermometric, Raman, and Laser Ablation Breakdown Spectroscopy Data and Major Composition of the Six Fluid Inclusion Types

	Microthermometric data (°C)					Raman (mol/kgH_2O)	LIBS (mol)		Major composition (wt %)		
FI type	T_e	$T_{m(ice)}$	$T_{s(hyd)}$	$T_{s(NaCl)}$	T_h	Cl^-	Na/Ca	Ca/Mg	NaCl	$CaCl_2$	$MgCl_2$
Lw_1	–45	–19.5	n.d.	No NaCl	nd	4.5	4.6	1.0	14	6	4
Lw_2	–58	n.d.	12.6	No NaCl	178.0	6.1	7.7	17.9	24	6	0.3
	n.d.	–25.0	9.0	No NaCl	164.8	6.0	3.0	No Mg	22	14	0
	n.d.	–24.6	8.7	No NaCl	165.7	6.0	3.7	12.2	23	12	0.9
Lwh	n.d.	–25.7	n.d.	132.3	172.8	6.5	3.8	No Mg	25	13	0
Lw'	no freezing	no freezing	n.d.	No NaCl	99.8	6.5	0.5	1.5	5	20	11.5
Lwh'	n.d.	–35.9	n.d.	140.7	140.8	6.5	0.8	1.7	8	19	9.5
Lw"	n.d.	–6.0	n.d.	n.d.	268.0°	2.2	3.7	24.0	9	5	0.1
	n.d.	–4.0	n.d.	n.d.	261.3°	1.2	5.0	No Mg	6	2.5	0

Notes: LIBS = laser-induced breakdown spectrosocpy; Lw_1, Lw_2, and Lwh = NaCl-rich brine; Lw' and Lwh' = $CaCl_2$-rich brine; Lw" = low-salinity fluid; T_e = eutectic temperature, $T_{m(ice)}$ = ice-melting temperature, $T_{m(hyd)}$ = hydrohalite melting temperature, $T_{s(NaCl)}$ = halite dissolution temperature, T_h = homogenization temperature (temperature of vapor phase disappearance); wt % = weight percent

transforms into halite at temperatures close to 10°C. This observation suggests that some of the metastable Lw_2 inclusions may transform into Lwh inclusions. The chlorinity, as deduced from Raman data, is 6 ± 0.5 mol/kg H_2O. The Na/Ca ratio ranges from 3 to 7.7, and the Ca/Mg ratio (in cases where magnesium was detected) ranges from 1 to 17.9. In Lw_1 and Lw_2 fluid inclusions from Qz4 trapped solids such as hematite, illite, kaolinite (identified by SEM analysis in opened fluid inclusions), chlorite, or dickite (identified by Raman microprobe) are common.

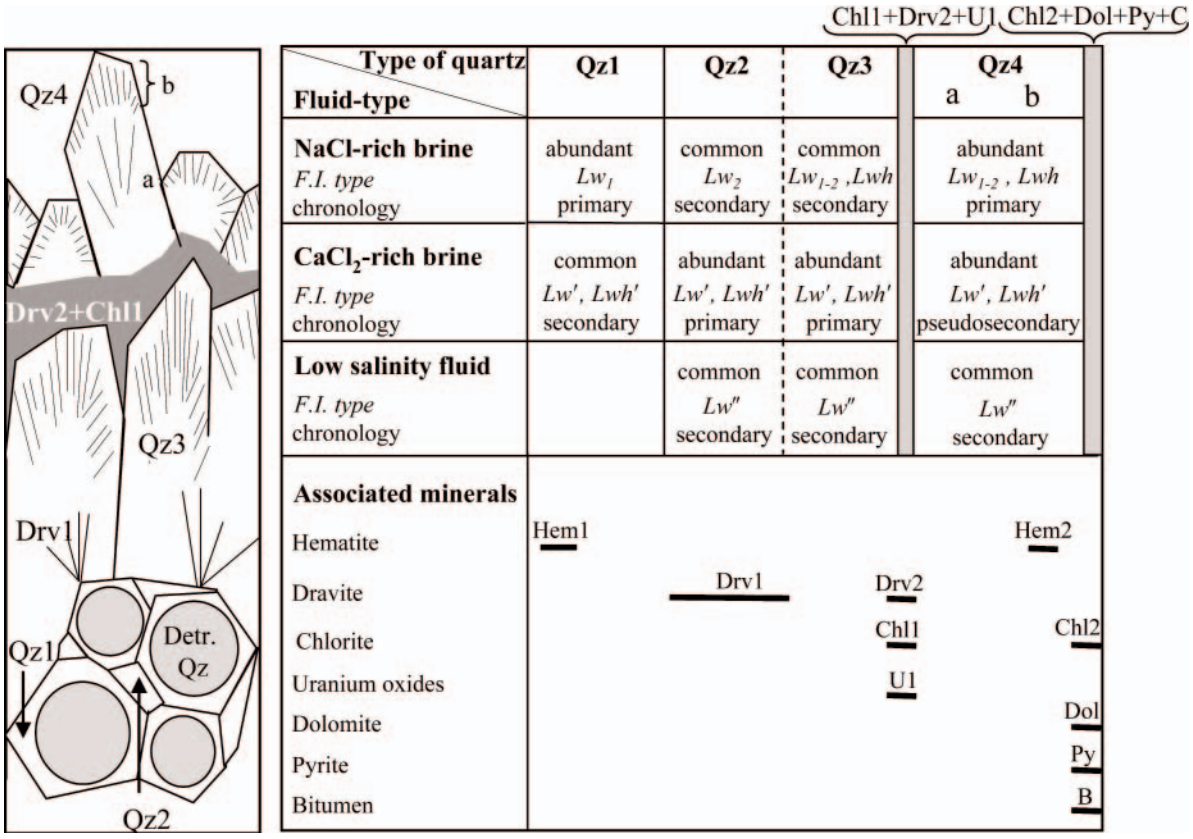


FIG. 6. Chronological and petrographic relationships between the different types of fluid inclusions and the sequence of minerals in the sandstones from the the McArthur River deposit. The relative abundance of each fluid type is given as a function of the quartz type in the paragentic sequence, with indication of the primary or secondary feature of the fluid inclusions and the type of associated mineral. For the quartz Qz4, two stages are distinguished: "a" corresponds to the first growth stage, and "b" to the late growth bands with abundant primary Lw_{1-2} and Lwh inclusions. Abbreviations: F.I. = fluid inclusion, Qz = quartz.

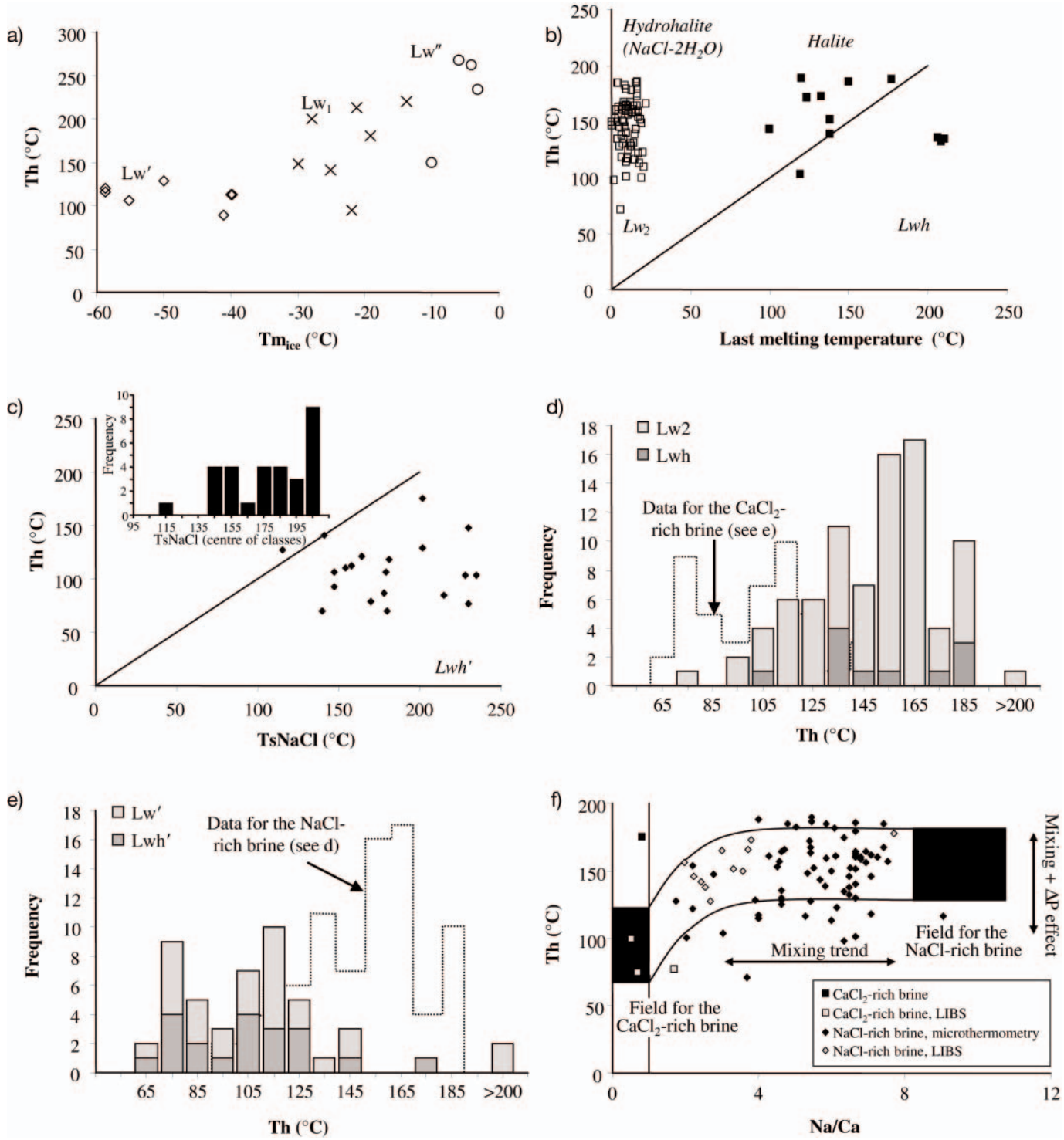


FIG. 7. Microthermometric data. (a). Homogenization temperature (T_h) vs. ice-melting temperature ($T_{m(ice)}$) diagram for the liquid-vapor fluid inclusions (Lw_1, Lw', and Lw", which correspond to the NaCl-, $CaCl_2$-rich brine, and low-salinity fluid, respectively). (b). T_h vs. T_m of the last solid phase for the NaCl-rich brine (Lw_2 and Lwh inclusions). (c) T_h vs. $T_{m(NaCl)}$ diagram and histogram of $T_{m(NaCl)}$ for the $CaCl_2$-rich Lwh' brine inclusions. (d). T_h histogram for the NaCl-rich Lw_2 and Lwh fluid inclusions. (e). T_h histogram for the $CaCl_2$-rich Lw' and Lwh' brine inclusions. (f). T_h vs. Na/Ca diagram for the NaCl- and $CaCl_2$-rich brine inclusions. Gray data points correspond to LIBS data, whereas black data points correspond to the estimates deduced from the phase transition temperatures in an H_2O-NaCl-$CaCl_2$ phase diagram. The fields corresponding to the predominant T_h values are reported for the NaCl- and the $CaCl_2$-rich brines.

Lwh fluid inclusions are similar to Lw_2 fluid inclusions but contain a halite cube. They mainly occur in Qz4 from the basement but also locally in Qz3 from the sandstone (Table 2). The $T_{m(ice)}$ ranges from –27.7° to –24.0°C, the $T_{m(hydrohalite)}$ from –3.2° to 19.2°C, the $T_{m\ (NaCl)}$ from 99.5° to 208°C (most data are below 180°C, Fig. 7b), and the T_h (temperature of vapor phase homogenization into the liquid phase) varies from 103.5° to 188°C (mode around 135°C, Fig. 7d).

The presence of halite in this type of fluid inclusion normally excludes the use of the Raman microprobe to determine chlorinity and LIBS for the cation ratio. However, one metastable fluid inclusion did not renucleate its halite cube immediately after cooling down to room temperature. This inclusion was analyzed by Raman and LIBS at room temperature before the halite cube reformed. This fluid inclusion has a chlorinity of 6.5 mol/kg H_2O and an Na/Ca ratio of 3.8. No Mg was detected. No gas was detected in Lwh fluid inclusions from the sandstone.

$CaCl_2$-rich brines

In Lw' and Lwh' inclusions (Fig. 5c, d), the liquid phase often failed to nucleate any ice or hydrate during cooling down to –190°C. Raman analyses at low temperature in these fluid inclusions showed a typical water spectrum. When ice finally nucleated, the eutectic temperature of Lw' and Lwh' inclusions was –70 ± 5°C. Lw' and Lwh' inclusions commonly have irregular shapes and sizes (generally <30 μm in length). The volume fraction of the vapor phase is <10 percent. Heterogeneously trapped hematite, kaolinite, and illite (identified by SEM) are common.

Lw' fluid inclusions mainly occur in Qz2 and Qz3 in the sandstone (Fig. 6) but also locally in secondary fluid inclusion planes in Qz1 from the sandstone and rarely in Qz4 from the basement (Table 2). Their $T_{m(ice)}$ values range from –58.8° to –30°C. T_h values mainly range from 58° to 137°C (Table 2, Fig. 7e), excluding some abnormally low and high T_h values (15°–50°C and >200°C) that probably result from posttrapping evolution (necking down). In some metastable fluid inclusions, a halite cube locally nucleates after the cooling tests, a behavior similar to that mentioned above for Lw_2 inclusions. Chlorinity is close to 6 mol/kg H_2O. Lw' fluid inclusions that are appropriate for LIBS analysis are rare because of the occurrence of trapped solid phases (Fig. 5c) or due to their small size (commonly <30 μm, Fig. 5f). Two inclusions were analyzed by LIBS and showed an Na/Ca ratio of 0.5 and 1.7, with no detectable Mg.

Lwh' fluid inclusions occur mainly in Qz2 and Qz3 (Fig. 6, Table 2) but also in fluid inclusion planes in Qz1 from the sandstone and as rare clusters in Qz4. The $T_{m(ice)}$ ranges from –58° to –36°C, and no hydrate melting was observed. The $T_{m(NaCl)}$ ranges from 115° to 235°C and is systematically higher than the homogenization temperature of vapor in the liquid phase (Fig. 7c). Homogenization (L + V→L) occurs between 63° and 175°C (Fig. 7c, e). The presence of halite in Lwh' inclusions made chlorinity measurements and LIBS analysis impossible, except for one fluid inclusion analyzed at room temperature before the nucleation of NaCl. This inclusion has a chlorinity of 6.5 mol/kg H_2O, an Na/Ca ratio of 0.8, and a Ca/Mg ratio of 1.7 (Table 2).

Low-salinity fluid

Lw" fluid inclusions consist of liquid and vapor with highly variable L/V ratios but lower than the L/V ratio of the brines (Fig. 5e). The $T_{m(ice)}$ values range from –1.6°C to –10.6°C (Fig. 7a, Table 2). The inclusions are usually 10 to 30 μm in size with an oval shape and contain trapped solid inclusions such as clays and carbonates (e.g., identified by Raman microspectroscopy in sample H459-33m). Lw" fluid inclusions have T_e values ranging from –53° to –35°C. These inclusions are rare and are mainly observed in the immediate vicinity of massive uranium orebodies. They occur as secondary fluid inclusion planes crosscutting the last growth band of Qz3 and as isolated fluid inclusions or as clusters in Qz4. Chlorinity deduced from Raman analysis of Lw" inclusions is close to 2 mol/kg H_2O. The Na/Ca ranges from 3.7 to 5, and the Ca/Mg ranges from 24 to higher values. The inclusions commonly did not homogenize prior to decrepitation because of the presence of radiolytic gases (H_2 and O_2 identified by Raman spectroscopy in the vapor phase of fluid inclusions). When the T_h was observed, most values were high (200°–250°C) and variable. The heterogeneity of the L/V ratios in a given fluid population is due to heterogeneous contents of H_2 and O_2, the amounts of which were qualitatively estimated by Raman spectroscopy by comparison between the relative peaks of gases (H_2 and O_2) and H_2O. These radiolytic gases are common in all types of fluid inclusions located very close to uranium mineralization, especially in postore quartz (Qz4). Details of the distribution of gases within the McArthur River deposit are given in Derome et al. (2003a) and are not discussed here.

Crush-leach analyses

Bulk crush-leach analysis was performed on quartz (Qz4) and dolomite from sample H459-33m and on quartz Qz4 from sample H273-103m. Samples were prepared and cleaned using the methods described by Banks et al. (2000). The anions Cl^- and Br^- were analyzed because halogens are conservative in solution and are not affected by fluid-rock interactions. Therefore, they represent the original composition of the paleofluids trapped in fluid inclusions. In sample H459-33m, Cl/Br ratios of 73 and 56 (by wt) were measured for Qz4 and dolomite, respectively. The Cl/Br ratio of Qz4 from sample H273-103m is 99. Such values are similar to the Cl/Br ratio of 55 obtained in a sample of euhedral quartz from the Rabbit Lake deposit by Pagel and Jaffrezic (1977) using neutron activation techniques.

Interpretation of Fluid Inclusion Data

Bulk salt content of brine inclusions

The composition of a representative set of the two fluid inclusion types was deduced from the combination of microthermometry and chlorinity and cation ratio data (Table 3). Chlorinity measurements from Raman microprobe analyses are fitted to the cation ratio deduced from LIBS analyses. The methodology used for the reconstitution of the bulk composition of an individual fluid inclusion from the combination of these techniques is described in Fabre et al. (2002). The data obtained from these analyses are plotted together with compositions deduced from phase transitions observed

during microthermometric measurements (Fig. 8). The characteristics of the two predominant fluid types are represented by two domains in Figure 8. The NaCl-rich brine inclusions can be divided into two groups: Lw_1 fluid inclusions that have a lower salinity than the Lw_2 and Lwh inclusions (about 20% salt chlorides, crosses in Fig. 8) and mainly correspond to fluids trapped in quartz overgrowths Qz1; and Lw_2 and Lwh fluid inclusions, with Na/Ca ratio of ~3 to 7.7 and salt content of ~30 to 38 percent (15–28 wt % NaCl + 2–13 wt % $CaCl_2$), that are mainly trapped in Qz3 and Qz4.

The $CaCl_2$-rich brine inclusions can also be divided into two groups: Lw' inclusions with an Na/Ca ratio of 0.5 to 1.7 and a salt content of ~30 percent (up to 5 wt % NaCl and 11.5 $MgCl_2$) according to the limited LIBS data); and Lwh' inclusions for which $T_{m(NaCl)}$ values are higher than T_h values and variable (Fig. 7c). The composition of the Lwh' inclusions is indicative of a fluid saturated with respect to halite at the trapping temperature, as the $T_{m\ (NaCl)}$ is highly variable and sometimes considerably higher than the T_h. According to the LIBS data obtained on the Lwh' fluid inclusion, the trapped brine contains 36.5 wt percent salt chlorides (8 wt % NaCl + 19 wt % $CaCl_2$ + 9.5 wt % $MgCl_2$; Table 3).

The NaCl- and $CaCl_2$-rich brines occur together in most of the studied samples. The NaCl-rich brine is the predominant fluid in Qz1 and Qz4, whereas the $CaCl_2$-rich brine predominates in Qz2 and Qz3 (Fig. 6, Table 2). This observation may indicate that two fluids from distinct reservoirs were successively injected at the base of the basin. Mixing between the NaCl- and the $CaCl_2$-rich brines is suggested by the range of Na/Ca ratios between 7.7 and 0.5 according to LIBS data (10.7–0.5 according to microthermometry). The NaCl-rich brine has the largest range from 7.7 down to 3 based on LIBS data and 10.7 down to 2 based on microthermometric data obtained on a greater number of fluid inclusions (Fig. 7f). Such a range can be interpreted as the result of the episodic mixing of the NaCl-rich brine with variable amounts of $CaCl_2$-rich brine (from 0–60%). The addition of a small amount of NaCl to a $CaCl_2$-rich brine leads to the saturation of the $CaCl_2$-rich brine with respect to halite, as shown by the H_2O-NaCl-$CaCl_2$ phase diagram (Fig. 8) and observed in the samples. This supports the hypothesis of mixing of the two brines within the studied area.

P-T conditions of trapping

Isochores have been drawn on the basis of the mean salt content and the T_h modes of the two fluid end members using the FLUIDS 1 package (Bakker, 2003) and the equations of Zhang and Frantz (1987).

The T_h modes of the NaCl-rich brine (135° and 165°C, Fig. 7d) are representative of the minimum trapping temperature of the regional basinal fluid, as the NaCl-rich brine is predominant in these quartz generations. The intersection of the isochores with the most probable thermal gradients (30, 35, and 40°C/km) yields two extreme P-T fields, depending on the fluid pressure regime (lithostatic or hydrostatic; Fig. 9). In both cases, at the lower intersections, the minimum fluid pressures yield a minimum depth estimate ranging from 4 to 5 km, assuming a mean value of the density of the sedimentary pile of 2.5 g/cm^3. At such depth, it is highly probable that pressure was lithostatic, as the transition between hydrostatic and lithostatic pressures occurs between 3 and 5 km. If a lithostatic pressure is considered, the intersection between the two main isochores and the 40°C/km gradient yields a temperature range of 190° to 235°C and a pressure range of 1,200 to 1,400 bars. Lower gradients yield temperatures and pressures which seem unrealistic for a basin where fluids

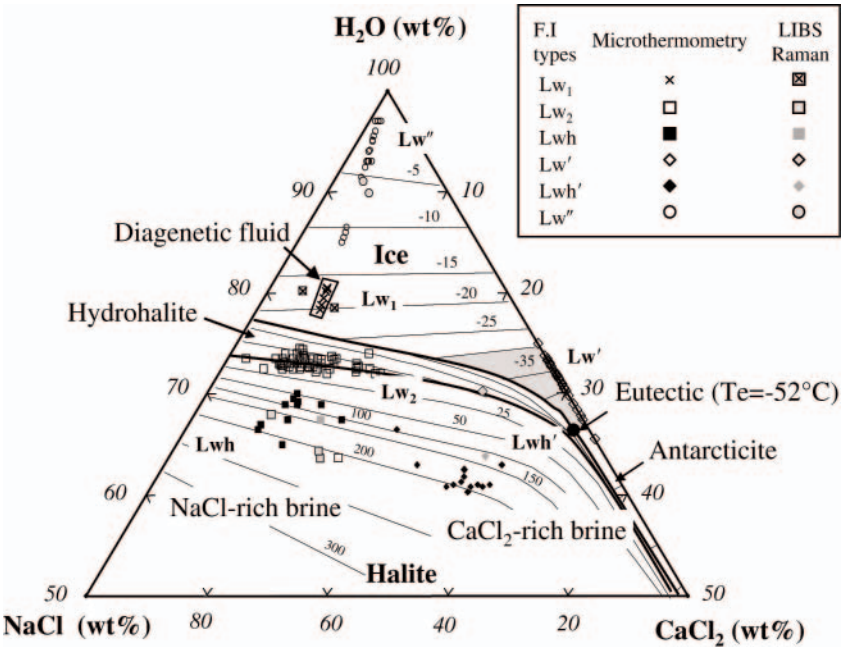


FIG. 8. H_2O-NaCl-$CaCl_2$ phase diagram with data points issued either from microthermometry or from combined Raman and LIBS analyses for all fluid inclusions types. This diagram shows that most fluid inclusions distribute within two main compositional fields (NaCl- and $CaCl_2$-rich brines) and that a series of data points correspond to a series of Lw_1 and Lw" inclusions (dilute fluids showing evidences of mixing or contamination with a more saline end member).

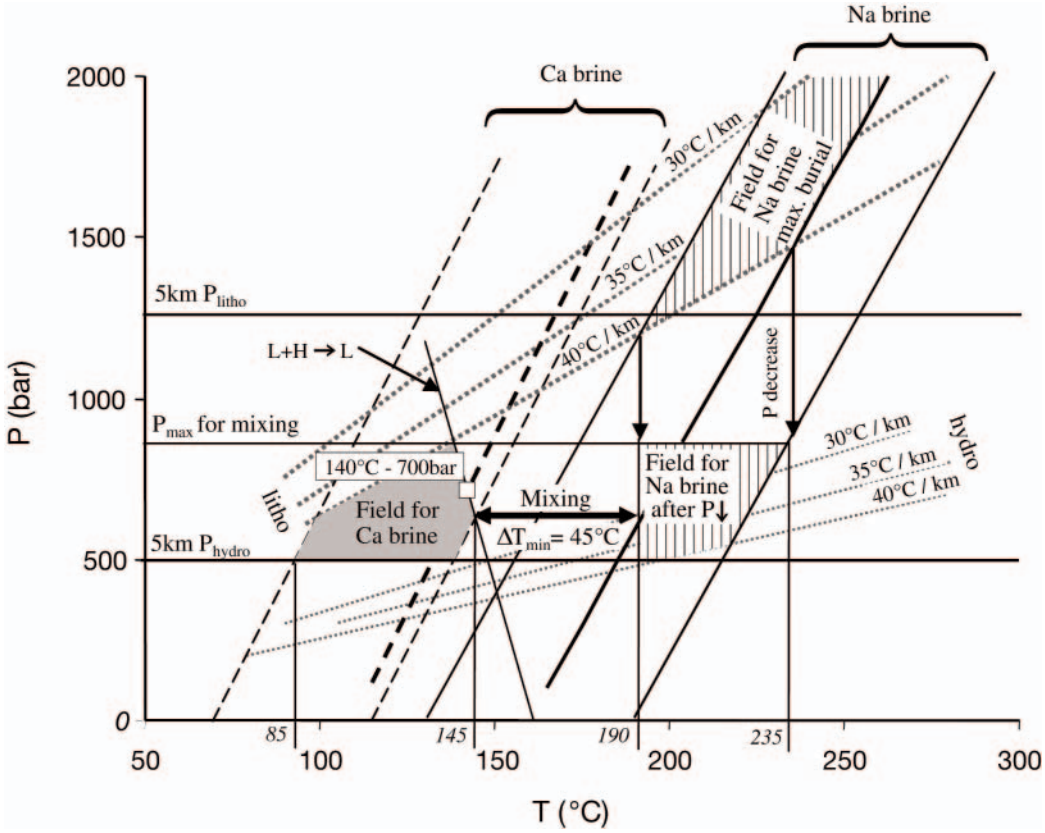


FIG. 9. P-T path model for the NaCl-rich brine and conditions of mixing with the $CaCl_2$-rich brine. Representative isochores (dashed lines) have been drawn for the main ranges of T_h for the two fluid types. The hydrostatic and lithostatic pressures at 5-km depth are reported as well as the hydrostatic and lithostaic gradients calculated for thermal gradients of 30°, 35°, and 40°C/km (dotted lines). The main P-T boxes representative of the trapping conditions of the early brines at the maximum of burial and the trapping of the two main brines are reported in gray.

were able to circulate. These estimates suggest a higher geothermal gradient than the 35°C/km determined at Rumple Lake by Pagel (1975b). A depth of about 5 km implies a denudation of the sedimentary cover of about 4.5 km from diagenesis to the present day in the McArthur River area. It is likely that the group of fluid inclusions (Lw_2, Lwh) with the highest T_h (165°–185°C) represent fluids trapped at a lower pressure (500–800 bars) but at temperature within the above defined range (190°–235°C; Fig. 9). A pressure decrease during the brecciation event is consistent with both tectonic activity inducing the formation of breccias and a drop to below lithostatic pressure (the minimum pressure being 500 bars if the pressure is hydrostatic; Fig. 9).

The $CaCl_2$-rich brine was saturated with respect to halite at the time of trapping. The halite dissolution curve for 30 wt percent NaCl (Bodnar and Vityk, 1994) has thus been plotted in the P-T diagram as a boundary (Fig 9). The isochores for these brines have been drawn by using FLUIDS 1 (Bakker, 2003). The T_h mode of the $CaCl_2$-rich brine in Qz3 (110° ± 5°C) is considered as the minimum temperature of the calcium-rich brine, as this is the dominant fluid in Qz3 (Table 2). The maximum field for the trapping conditions of the $CaCl_2$-rich brine is limited by three boundaries: the isochores, the minimum pressure deduced from the P-T conditions of trapping of the NaCl-rich brine at hydrostatic conditions (500 bars; Fig. 9), and the halite saturation curve. Considering that the mean isochore is the most representative of the $CaCl_2$-rich brine, the most likely trapping conditions are given by the intersection of this isochore with the halite dissolution curve (~140°C and ~700 bars).

The two brines mixed in breccia bodies, as shown by the variations of Na/Ca ratios (Fig. 7f), at pressures close to the hydrostatic pressure. The P-T diagram (Fig. 9) shows that the mixing was necessarily nonisothermal. The $CaCl_2$-rich brine was probably at least 30° to 50°C cooler than the NaCl-rich brine.

Significance of the H_2-O_2-rich low-salinity fluid

A hydrogen- and oxygen-rich, low-salinity fluid, represented by Lw" inclusions, is characterized by much lower chloride concentrations than the brines (Fig. 8, Table 3). This fluid is locally found in clusters of inclusions or in fluid inclusion planes, mostly at the contact or in close proximity to the uranium ores (< ~10 m). The P-T conditions of trapping of this fluid could not be established because of the high variability in T_h, due to the heterogeneous trapping of H_2 and O_2. These gases are typical of radiolysis of water at the contact with uranium minerals (Dubessy et al., 1988). The occurrence of such gases indicates that the low-salinity fluid was in contact with some significant uranium mineralization,

suggesting that this Lw" fluid circulated after the first stages of uranium deposition. Such a low-salinity fluid was also described in the vicinity of uranium deposits from the Kombolgie basin (Northern Territories, Australia; Derome et al., 2003b), where it was interpreted as a hot, basement-derived fluid, responsible for the reduction of uranium by mixing with the basinal brines. However, at McArthur River, Saskatchewan, the low-salinity fluid occurs in fluid inclusion planes crosscutting Qz3 or as clusters in postore Qz4. Since this fluid shows no indication of having mixed with the brines and since it always contains high amounts of H_2 and O_2 in the vapor phase, it is considered as having circulated later than the brines and after uranium ore was formed and is, therefore, unrelated to mineralization. This situation differs from the Australian deposits, where dilute fluids mixed with brines and thereby caused the formation of uranium ores (Derome et al., 2003b).

Discussion

Origin of fluids

Two brines of contrasting Na/Ca ratio were simultaneously trapped in quartz that cements the breccias (Qz3 and Qz4) in both the basement and the overlying sandstones. Both brines have very high chloride content (up to 7 mol/kg H_2O). The chlorine enrichment in the dominant NaCl-rich brine, which reaches 35 wt percent chloride salts, may have resulted from a number of different processes: (1) water uptake during hydration of anhydrous minerals, such as feldspars, was extremely limited in the Athabasca sediments as detrital feldspars are very rare; (2) dissolution of halite also is ruled out, as the Cl/Br ratio of the brine (between 73 and 100 in wt, at McArthur River) is much lower than Cl/Br of seawater (around 300, Fontes and Matray, 1993) or waters having leached halite; (3) membrane filtration effects are not efficient enough to increase the Cl content to saturation with respect to halite and to such low Cl/ Br ratios; and (4) the expulsion of a residual primary brine from evaporite layers is the most likely origin since evaporitic sediments are known in the Douglas and Carswell Formations (Ramaekers, 1990). This is confirmed by the low Cl/Br ratio obtained on two Qz4 samples from McArthur River. A contribution of Br from organic matter, proposed by Pagel and Jaffrezic (1977) to explain such a low Cl/Br ratio, is at the moment unverified (Hanor, 1994; Yardley et al., 2000). The salt content and the low Cl/Br ratio, therefore, favor the expulsion of primary brines from evaporitic layers.

The origin of the $CaCl_2$-rich brine is more difficult to explain. Such brines have been observed in two other Proterozoic basins (Franceville basin: Mathieu, 1999; Kombolgie sub-basin: Derome et al., 2003b). They also occur in Silurian strata from the Michigan basin (Wilson and Long, 1993; Davisson and Criss, 1996). Such high calcium contents may result from the interaction between NaCl-rich diagenetic brines and Ca-rich rocks (Wilson and Long, 1993; Hanor, 1994; Davisson and Criss, 1996). Interactions of NaCl-rich brines with Ca-rich lithologies (e.g., plagioclase-, pyroxene-, amphibole-bearing rocks in basement lithologies) is thus the most likely explanation for the $CaCl_2$-rich brines observed at McArthur River. The Ca enrichment of the basinal brine at McArthur River probably occurred during circulation from shallow levels down to basement, along and below the unconformity.

Paleofluid regime in the vicinity of the P2 orebody

According to petrographic relationships, the NaCl-rich brine is the earliest basinal fluid in the McArthur River area and was still present during and after uranium deposition (Table 2, Fig. 10). The NaCl-rich brine was the regional basinal fluid, as it has been observed everywhere in the Athabasca basin (Rumple Lake and Cluff Lake: Pagel, 1975b; Rabbit Lake: Pagel and Jaffrezic, 1977; Derome, 2002; Shea Creek: Derome, 2002). A cooler NaCl-rich brine, from the upper levels of the Athabasca basin percolated into the basement lithologies, where Na was exchanged with Ca to form the $CaCl_2$-rich brine (Fig. 10b). As pressure decreased, the $CaCl_2$-rich brine moved into the sandstone (and was trapped as inclusions in the pervasive silicification, Qz2, as well as in Qz3 from the breccia bodies; Table 2, Fig. 10b), where it mixed with the NaCl-rich brine. The predominance of the $CaCl_2$-rich brine in Qz2 and Qz3 suggests that this brine was injected into fault zones after the Qz1 stage (where the NaCl-rich brine is dominant) and that the $CaCl_2$-rich brine was the main fluid present during the growth of Qz2 and Qz3. Thereafter, the NaCl-rich brine was the dominant fluid in quartz Qz4, suggesting that the availability of $CaCl_2$-rich brine decreased during the growth of Qz4. We conclude the calcic-brine episode is characteristic of the pre- to synore Qz2 and Qz3 cementation events (Figs. 3, 4). This calcic-brine episode may have played a key role in the process of uranium mobilization and transportation, but the evolution of the oxidation state could not be constrained from the present study.

Summary and Conclusions

The present study shows that the nature and timing of fluid percolation within faults and at the unconformity controlled the genesis of the P2 uranium orebody. Two main types of brines are distinguished for the first time in the Athabasca sandstones and the underlying basement in the vicinity of uranium mineralization: a hot (min 190°C) NaCl-rich brine (about 25 wt % NaCl + up to 14 wt % $CaCl_2$ + 1 wt % $MgCl_2$) and a cooler (approx 140°C) $CaCl_2$-rich brine (5–8 wt % NaCl + up to 20 wt % $CaCl_2$ + up to 11 wt % $MgCl_2$). Previous workers (Pagel, 1975b; Pagel and Jaffrezic, 1977; Kotzer and Kyser, 1995) considered only one type of brine circulating at a temperature of about 200°C. Quartz cementation at the base of the Athabasca basin occurred in three stages with an early diagenetic cementation associated with the NaCl-rich basinal brine (Fig. 10a); a later cementation (Qz2-Qz3), corresponding to a first brecciation event, was synchronous with the input of the $CaCl_2$-rich brine (Fig. 10b). This calcic-brine episode may have been related to reactivation of basement faults, such as the P2 structure. The third step of cementation followed a second brecciation event and is represented by the postore Qz4 quartz crystals in which the NaCl-rich brine is again dominant (Fig. 10c). The two brines show evidence of mixing, especially in quartz Qz3. This quartz commonly hosts dravite (Drv1) and predates the chlorite-dravite (Drv2) brecciation event related to the main uranium mineralization event, as shown by the petrographic study and in accordance

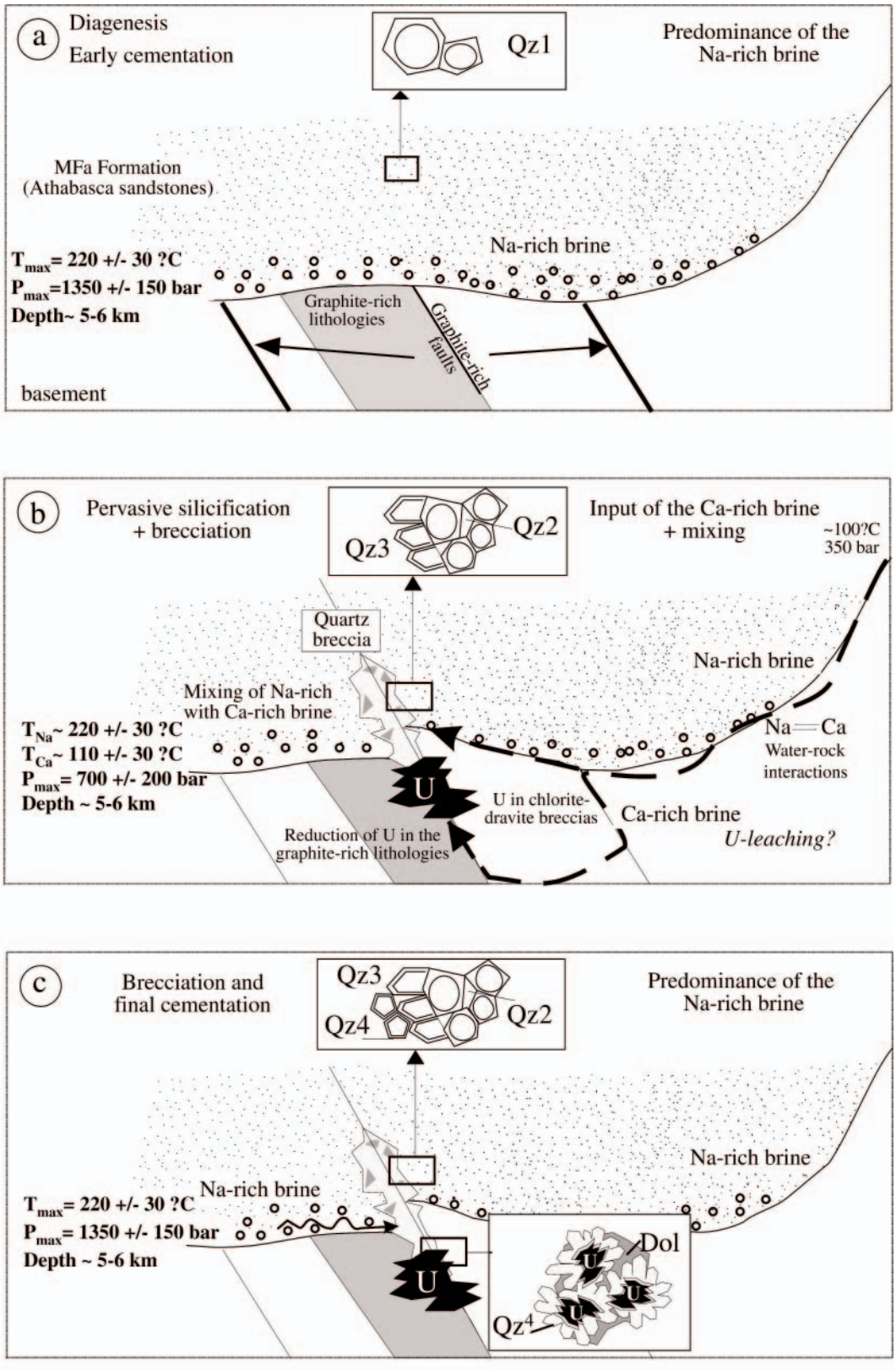


FIG. 10. Schematic representation of fluid circulation and P-T conditions that prevail at the base of the basin at each step of quartz cementation in the McArthur River deposit area and its possible link with the genesis of U mineralization. (a). Early cementation at the bottom of the sandstone formation. (b). Interactions of the Na-rich brine with Ca-rich lithologic units and formation of a Ca-rich brine which subsequently mixed with main Na-rich brines along fault zones (uranium deposition stage). (c). Final cementation of breccias by Na-rich brines.

with previous results (McGill et al., 1993; Kotzer and Kyser, 1995; Fayek and Kyser, 1997). According to most of the petrographic and paragenetic studies that have been carried out in the McArthur River deposit, euhedral quartz (Q2 of Kotzer and Kyser, 1995, Fayek and Kyser, 1997, and Q1 of Alexandre et al., 2003) is considered as postore. However, the present petrographic and fluid inclusion study has shown the existence of two generations of euhedral quartz, Qz3 and Qz4. The main stage of uranium deposition postdated the Qz2 stage and was probably synchronous with or immediately postdated the Qz3 stage and predated the Qz4 quartz cementation stage. Therefore, the two brines (NaCl- and $CaCl_2$-rich brines), which were the dominant fluids trapped in Qz3 and Qz4, can be considered as representative of the main fluid types that circulated during the formation of uranium ores.

The chloride content of the NaCl-rich brine reaches 6.5 mol Cl^-/kg H_2O, and its Cl/Br ratio suggests that it was expelled from evaporitic layers and can be considered as a primary evaporitic brine. The NaCl-rich brine dominates over a large range of depths and laterally over distances of several hundreds of kilometers (e.g., Rumple Lake and Cluff Lake: Pagel, 975b; Rabbit Lake: Pagel and Jaffrezic, 1977; Pagel et al., 1980; Shea Creek prospect: Derome, 2002), suggesting a huge saline fluid reservoir at the scale of the basal sandstone formation within the Athabasca basin. The Ca enrichment resulted from fluid-rock interactions during the infiltration of the NaCl-rich brine into the basement lithological units.

The minimum P-T conditions during the maximum burial of the sandstones were 1,200 to 1,400 bar (5 km) and 190° to 235°C. In response to tectonic movement and breccia formation, the pressure decreased and enabled the $CaCl_2$-rich brine (approx 140°C) to enter the fluid system and to mix with the resident warmer basinal NaCl-rich brine (min 190°C) in the breccia bodies. This critical change in the fluid regime is probably linked to major changes in the tectonic regime during a world-wide geodynamic event. The fragmentation of the supercontinent Columbia, associated with the development of anorogenic magmatism and continental rifting, which began at 1.6 Ga and continued until its final breakup at about 1.2 Ga (Condie, 2002; Rogers and Santosh, 2002; Zhao et al., 2004), represents a major geodynamic event that may have been responsible for a critical change in fluid regime in the Athabasca basin, linked to the formation of uranium mineralization in the McArthur River area.

Acknowledgments

The COGEMA Company is gratefully acknowledged for financial support of this study, for the technical and scientific assistance during sampling, and for giving the permission for publishing the results. CAMECO Company is also greatly thanked for giving the permission for sampling and for the results to be published. All the members of the East Athabasca Modeling Project are also thanked for their discussions and comments. The authors gratefully acknowledge E. Spooner, K. Kyser, G. Spry, and M. Hannington for their fruitful comments and advice during the review of the paper.

August 28, 2003; December 2, 2005

REFERENCES

Alexandre, P., and Kyser, K., 2003, Geochronology of the Paleoproterozoic basement-hosted unconformity-type uranium deposits in northern Saskatchewan, Canada: International Conference on Uranium Geochemistry, Nancy, 2003, Unité de recherche G2R (Géologie et Gestion des Matières Premières Minerales et Energétiques), Proceedings, p. 37–40.

Alexandre, P., Kyser, K., and Polito, P., 2003, Mineralogy, fluid geochemistry and evolution of Paleoproterozoic basement hosted unconformity-type uranium deposits in northern Saskatchewan, Canada: International Conference on Uranium Geochemistry, Nancy, 2003, Unité de recherche G2R (Géologie et Gestion des Matières Premières Minerales et Energétiques), Proceedings, p. 41–44.

Annesley, I.R., and Madore, C., 2002, Thermotectonics of Archean/Paleoproterozoic basement to the eastern Athabasca unconformity-type uranium deposits, *in* Kribek, B., and Zeman, J., eds., Uranium deposits: From their genesis to their environmental aspects: Prague, Czech Geological Survey, p. 33–36.

——2003, Wollaston-Mudjatik transition zone: Its characteristics and influence on the genesis of unconformity-type uranium deposits: International Conference on Uranium Geochemistry, Nancy, 2003, Unité de recherche G2R (Géologie et Gestion des Matières Premières Minerales et Energétiques), Proceedings, p. 55–58.

Annesley, I.R., Madore, C., and Portella, P., 2001, Paleoproterozoic structural, metamorphic, and magmatic evolution of the eastern sub-Athabasca basement: Controls on unconformity-type uranium deposits [ext. abs.], *in* Williams, P.J., ed., A hydrothermal odyssey: Townsville, Queensland, James Cook University, Extended Conference Abstracts, p. 3–4.

Armstrong, R.L., and Ramaekers, P., 1985, Sr isotopic study of Helikian sediment and diabase in the Athabasca basin, northern Saskatchewan: Canadian Journal of Earth Sciences, v. 22, p. 399–407.

Armstrong, R.L., Quirt, D., and Hoeve, J., 1988, Rb-Sr dating of diabase dike in the Athabasca basin, northern Saskatchewan: Saskatchewan Research Council Publication R-855-3-7-88, 21 p.

Bakker, R.J., 2001, Combined Raman spectroscopy and low temperature microthermometry: European Current Research on Fluid Inclusions (ECROFI), 16th, Porto, 2001, Porto University, Proceedings, p. 15–18.

——2003, Package *FLUIDS* 1. Computer programs for analysis of fluid inclusion data and for modelling bulk fluid properties: Chemical Geology, v. 194, p. 3–23.

Banks, D.A., Green, R., Cliff, R.A., and Yardley, B.W. D., 2000, Chlorine isotopes in fluid inclusions: Determination of the origins of salinity in magmatic fluids: Geochimica et Cosmochimica Acta, v. 64, p. 1785–1789.

Bodnar, J.R., and Vityk, M.O., 1994, Interpretation of microthermometric data for H_2O-NaCl fluid inclusions, *in* De Vivo, B., and Frezzotti, M.L., ed., Fluid inclusions in minerals: Methods and applications: Blacksburg, Virginia, Virginia Tech, p. 117–130.

Chiarenzelli, J., Aspler, L., Villeneuve, M., and Lewry, J., 1998, Early Proterozoic evolution of the Saskatchewan craton and its allochtonous cover, Trans-Hudson orogen: Journal of Geology, v. 106, p. 247–267.

Condie, K.C., 2002, Breakup of a Paleoproterozoic supercontinent: Gondwana Research, v. 5, p. 41–43.

Cumming, G.L., and Krstic, D., 1992, The age of unconformity-related uranium mineralization in the Athabasca basin, northern Saskatchewan: Canadian Journal of Earth Sciences, v. 29, p. 1623–1639.

Davisson, L.M., and Criss, R.E., 1996, Na-Ca-Cl relations in basinal fluids: Geochimica et Cosmochimica Acta., v. 60, p. 2743–2752.

Derome, D., 2002, Evolution et origine des saumures dans les bassins protérozoïques au voisinage de la discordance socle/couverture. L'exemple de l'environnement des gisements d'uranium associés aux bassins Kombolgie (Australie) et Athabasca (Canada): Unpublished Ph.D. thesis, Nancy, Université Henri Poincaré, 232 p.

Derome, D., Cathelineau, M., Cuney, M., and Lhomme, T., 2003a, Fluid inclusion evidence of the differential migration of H_2 and O_2 in the McArthur River unconformity-type uranium deposit (Saskatchewan, Canada). Possible role on the host rock alteration: Journal of Geochemical Exploration, v. 78–79, p. 525–530.

Derome, D., Cuney, M., Cathelineau, M., Fabre, C., Dubessy, J., Bruneton, P., and Hubert, A., 2003b, A detailed fluid inclusion study in silicified breccias from the Kombolgie sandstones (Northern Territory, Australia): Inferences for the genesis of middle-Proterozoic unconformity-type uranium deposits: Journal of Geochemical Exploration, v. 80, p. 259–275.

Dubessy, J., Audeoud, D., Wilkins, R., and Kosztolanyi, C., 1982, The use of the Raman microprobe mole in the determination of the electrolytes

dissolved in the aqueous phase of fluid inclusions: Chemical Geology, v. 37, p. 137–150.

Dubessy, J., Pagel, M., Beny, J. M., Christensen, H., Hickel, B., Kosztolanyi, C., and Poty, B., 1988, Radiolysis evidenced by H_2-O_2 and H_2-bearing fluid inclusions in three uranium deposits: Geochimica et Cosmochimica Acta, v. 52, p. 1155–1167.

Dubessy, J., Poty, B., and Ramboz, C., 1989, Advances in C-O-H-N-S fluid geochemistry based on micro-Raman spectrometric analyses of fluid inclusions: European Journal of Mineralogy, v. 1, p. 517–534.

Dubessy, J., Lhomme, T., Boiron, M.C., and Rull, F., 2002, Determination of chlorinity in aqueous fluids using Raman spectroscopy of the stretching band of water at room temperature: Application to fluid inclusions: Applied Spectroscopy, v. 56, p. 99–106.

Fabre, C., Boiron, M.C., Dubessy, J., and Moissette, A., 1999, Determination of ions in individual fluid inclusions by laser ablation optical emission spectroscopy: Development and applications to natural fluid inclusions: Journal of Analytical Atomic Spectrometry, v. 14, p. 913–922.

Fabre, C., Boiron, M.C., Dubessy, J., Cathelineau, M., and Banks, D.A., 2002, Paleofluid chemistry of a single fluid event: A bulk in-situ multi-technique analysis (LIBS, Raman spectroscopy) of an Alpine fluid (Mont-Blanc): Chemical Geology, v. 182, p. 249–264.

Fayek, M., and Kyser, T.K., 1997, Characterization of multiple fluid-flow events and rare-earth-element mobility associated with formation of unconformity-type uranium deposits in the Athabasca basin, Saskatchewan: Canadian Mineralogist, v. 35, p. 627–658.

Fayek, M., Kyser, T.K., and Riciputi, L.R., 2002, U and Pb isotope analysis of uranium minerals by ion-microprobe and the geochronology of the McArthur River and Sue zone uranium deposits, Saskatchewan Canada: Canadian Mineralogist, v. 40, p. 1717–1733.

Fontes, J.C., and Martray, J.M., 1993, Geochemistry and origin of formation brines from the Paris basin, France. 1. Brines associated with Triassic salts: Chemical Geology, v. 109, p. 149–175.

Goldstein, R.H., and Reynolds, T.J., 1994, Systematics of fluid inclusions in diagenetic minerals. Society of Economic Paleontologists and Mineralogists (SEPM) Short Course Volume 31, 198 p.

Hanor, J.S., 1994, Origin of saline fluids in sedimentary basins: Geological Society Special Publication 78, p. 151–174.

Heine, T.H., 1986, The geology of the Rabbit Lake uranium deposit, Saskatchewan: Canadian Mineralogist, v. 33, p. 134–143.

Hoeve, J., and Quirt, D., 1984, Mineralization and host rock alteration in relation to clay mineral diagenesis and evolution of the middle Proterozoic Athabasca basin, northern Saskatchewan, Canada: Saskatchewan Research Council Technical Report 187, 187 p.

——1987, A stationary redox front as a critical factor in the formation of high grade, unconformity-type uranium ores in the Athabasca basin, Saskatchewan, Canada: Bulletin Minéralogie, v. 110, p. 151–171.

Hoeve, J., and Sibbald, T.I.I., 1978, On the genesis of Rabbit Lake and other unconformity-type uranium deposits in northern Saskatchewan, Canada: Economic Geology, v. 73, p. 1450–1473

Hoffman, P., 1990, Subdivision of the Churchill province and extend of the Trans-Hudson orogen: Geological Association of Canada Special Paper 37, p. 15–39.

Knipping, H.D., 1974, The concepts of supergene versus hypogene emplacement of uranium at Rabbit Lake, Saskatchewan, Canada: International Atomic Energy Agency (IAEA), Formation of Uranium Deposits Symposium, Athens, 6–10 May, Vienna, Proceedings, p. 531–548.

Komninou, A., and Sverjensky, D.A., 1996, Geochemical modeling on the formation of an unconformity-type uranium deposit: Economic Geology, v. 91, p. 590–606.

Kotzer, T.G., and Kyser, T.K., 1995, Petrogenesis of the Proterozoic Athabasca basin, northern Saskatchewan, Canada, and its relation to diagenesis, hydrothemal uranium mineralization and paleohydrogeology: Chemical Geology, v. 120, p. 45–89.

Kotzer, T.G., Kyser, T.K., and Irving, E., 1992, Paleomagnetism and the evolution of fluids in the Proterozoic Athabasca basin, northern Saskatchewan, Canada: Canadian Journal of Earth Sciences, v. 29, p. 1474–1491.

LeCheminant, A.N., and Heaman, L.M., 1989, McKenzie igneous events, Canada: Middle Proterozoic hotspot magmatism associated with ocean opening: Earth and Planetary Science Letters, v. 96, p. 38–48.

Little, H.W., 1974, Uranium in Canada: Geological Survey of Canada, Report of Activities, Pt. A, 74–1, p. 137–139.

Lorilleux, G., Jébrak, M., Cuney, M., and Baudemont, D., 2002, Polyphase hydrothermal breccia associated with unconformity-related uranium mineralizations (Canada): From fractal analysis to structural significance: Journal of Structural Geology, v. 24, p. 223–238.

Madore, C., Annesley, I.R., and Tran, H.T., 1999, Petrology and geochemistry of Paleoproterozoic Wollaston Group metasediments from the eastern Keller Lake-Siemens Lake area, Saskatchewan: A preliminary interpretation: Saskatchewan Geological Survey, Summary of Investigations, v. 2, p. 80–89.

Mathieu, R., 1999, Reconstitution des paleocirculations fluides et des migrations élémentaires dans l'environnement d'Oklo (Gabon) et des argilites de Tournemire (France): Unpublished Ph.D. thesis, Nancy, Institut National Polytechnique de Lorraine, 518 p.

Matthews, R., Koch, R., and Leppin, M., 1997, Advances in integrated exploration for unconformity uranium deposits in western Canada: Exploration 97, International Conference on Mineral Exploration, 4th Decennial, Toronto, Canada, Proceedings, p. 993–1024.

McGill, B.D., Marlatt, R.B., Matthews, R.B., Sopuck, V.J., and Homeniuk, L.A., 1993, The P2 north uranium deposit, Saskatchewan, Canada: Exploration and Mining Geology, v. 2, p. 321–331.

Mernagh, T.P. and Wilde, A.R., 1989, The use of the laser Raman microprobe for the determination of salinity in fluid inclusions: Geochimica et Cosmochimica Acta, v. 53, p. 765–771.

Oakes, C.S., Bodnar, R.J., and Simonson, J.M., 1990, The system NaCl-$CaCl_2$-H_2O: I. The ice liquidus at 1 atm total pressure: Geochimica et Cosmochimica Acta, v. 54, p. 603–610.

Pagel, M., 1975a, Cadre géologique des gisements d'uranium dans la structure Carswell (Saskatchewan, Canada)-"Etude des phases fluides:" Unpublished Ph.D. thesis, Nancy University, 157 p.

——1975b, Détermination des conditions physico-chimiques de la silicification diagénétique des grès Athabasca (Canada) au moyen des inclusions fluides: Comptes Rendus Académie Sciences Paris, v. 280, p. 2301–2304.

Pagel, M., and Jaffrezic, H., 1977, Analyses chimiques des saumures des inclusions du quartz et de la dolomite du gisement d'uranium de Rabbit Lake (Canada). Aspect méthodologique et importance génétique: Comptes Rendus Académie Sciences Paris, v. 284, p. 113–116.

Pagel, M., Poty, B., and Sheppard, M. F. S., 1980, Contribution to some Saskatchewan uranium deposits mainly from fluid inclusion and isotopic data, *in* J. Ferguson and A. Goleby, eds, Uranium in the Pine Creek Geosyncline: Vienna, International Atomic Energy Agency (IAEA), p. 639–645.

Quirt, D., 2000, Sub-Athabasca Group fanglomerate in the McArthur River-Read Lake area, Saskatchewan: GeoCanada 2000: The millenium geoscience summit [abs.]: Geological Association of Canada, Mineralogical Association Canada (GAC-MAC), Joint Annual Meeting, Calgary, Abstract 251.

Ramaekers, P., 1990, Geology of the Athabasca Group (Helikian) in northern Saskatchewan: Saskatchewan Energy and Mines, Saskatchewan Geological Survey, Report 195, 49 p.

Roedder, E., 1984, Fluid inclusions: Reviews in Mineralogy, v. 12, 644 p.

Rogers, J.J.W., and Santosh, M., 2002, Configuration of Columbia, a Mesoproterozoic supercontinent: Gondwana Research, v. 5, p. 5–22.

Ruzicka, V.,1986, Uranium deposits in the Rabbit Lake-Collins Bay area, Saskatchewan, Canada: Canadian Institute of Mining Metallurgy and Petroleum Special Volume 33, p. 144–149.

Thomas, D., Matthews, R.B., and Sopuck, V., 2000, Athabasca basin (Canada) unconformity-type uranium deposits: Exploration model, current mine developments and exploration directions: Geology and Ore deposits 2000: The Great Basin and Beyond: Geological Society of Nevada Symposium, May 15–18, 2000, Proceedings, v. 1, p.103–125.

Wilson, M.R., and Kyser, T.K., 1987, Stable isotope geochemistry of alteration associated with the Key Lake uranium deposit, Canada: Economic Geology, v. 82, p. 1540–1557.

Wilson, T.P., and Long, D.T., 1993, Geochemistry and isotope chemistry of Ca-Na-Cl brines in the Silurian strata, Michigan basin, U.S.A.: Applied Geochemistry, v. 8, p. 507–524.

Yardley, B.W.D., Banks, D.A., and Barnicoat, A.C., 2000, The chemistry of crustal brines: Tracking their origins, *in* Porter, T.M., ed., Hydrothermal iron oxide copper gold and related deposits: A global perspective: Australian Mineral Foundation, p. 61–70.

Zhang, Y.G., and Frantz, J.D., 1987, Determination of the homogenization temperatures and densities of supercritical fluids in the system NaCl-KCl-$CaCl_2$-H_2O using synthetic fluid inclusions: Chemical Geology, v. 64, p. 335–350.

Zhao, G., Sun, M., Wilde, S.A., and Sanzhong, L., 2004, A Paleo-Proterozoic supercontinent: Assembly, growth and breakup: Earth-Sciences Reviews, v. 67, p. 91–123.